Journal of Ceramic Processing Research. Vol. 10, No. 4, pp. 512~520 (2009)

J O U R N A L O F
Ceramic Processing Research

Synthesis and characterization of Rh/Al_2O_3-CeO_2 catalysts: effect of the Ce^{4+}/Ce^{3+} ratio on the MTBE removal

Ignacio Cuauhtémoc[a], Gloria Del Angel[a,*], Gilberto Torres[b], Juan Navarrete[c], Carlos Angeles-Chavez[c] and Juan Manuel Padilla[a]

[a]*Universidad Autónoma Metropolitana–Iztapalapa, Departamento de Química, Av. San Rafael Atlixco 186, C.P. 09340; P.O. Box 55–534 México D.F., Mexico*

[b]*Universidad Juárez Autónoma de Tabasco, DACB, Km 1 carretera Cunduacàn-Jalpa de Menedez A.P. 24, Cunduacan, Tabasco C.P. 86690, México*

[c]*Instituto Mexicano del Petróleo, Eje Central Lázaro Cárdenas 152, AP. 14–805, C.P. 07730, México DF., México*

Rhodium supported catalysts were prepared by impregnating γ-Al2O-Ce supports, which were prepared from boehmite and cerium nitrate with different cerium contents (1, 5, 10 and 20 Ce wt%). High specific surface areas, which diminish with the cerium content, were obtained. At high cerium contents the X-ray Diffraction (XRD) patterns showed the characteristic peaks of cerium oxide. X-ray photoelectron Spectroscopy (XPS) identified the presence of Rh^0 and $Rh^{\delta+}$ on the catalysts. The analysis of the Ce 3d region showed the presence of Ce^{3+} and Ce^{4+} where their relative abundance depends on the cerium content. Small rhodium particle sizes were determined by High Angle Annular Dark Field (HAADF) Scanning Transmission Electron Microscopy (STEM). It has been found that the conversion for the wet oxidation of methyl *tert*-butyl ether (MTBE) depends on the cerium content; conversion ranging from 73 to 96% were reached. A correlation between the total mineralization of MTBE and the relative abundance of the Ce^{4+}/Ce^{3+} ratio was observed. A total mineralization, as high as 87%, was obtained in the catalyst with the highest Ce^{4+}/Ce^{3+} ratio.

Key words: Rhodium alumina-ceria catalysts; MTBE wet oxidation; Rhodium XPS spectra; Alumina-ceria catalysts; MTBE mineralization; Rhodium HAADF-STEM.

Introduction

Methyl *tert*-butyl-ether (MTBE) has been used for two decades as an oxygenated compound to improve the octane number in the gasoline pool formulation [1, 2]. However, the extensive use of MTBE has generated significant environmental problems. MTBE is extremely soluble in water and it has been reported as an important pollutant in groundwater and surface water [3]. MTBE is highly resistant to being decomposed, it is a very slowly biodegraded compound; hence, contaminated water must be purified by cutting-edge technologies. Catalytic Wet Air Oxidation (CWAO) is a technique that is suitable to destroy pollutants such as phenols, carboxylic acids, industrial wastewater, etc [4, 5]. The main advantage of this method of treatment is the high mineralization (conversion to CO_2) of organic pollutants into effluents. The catalysts that are more frequently reported for CWAO use noble metals supported on a large number of mineral oxides such as: Al_2O_3 [6], CeO_2 [7-10], TiO_2 [11, 12], ZrO_2 [13] and ZnO-Al_2O_3 [14, 15].

In particular, rhodium supported on CeO2 has been reported as an efficient gas phase oxidation catalyst for organic compounds. Its performance is attributed to the formation of the Ce^{3+}/Ce^{4+} pair, since the oxidation and reduction cycles are important for the storage and oxygen supply during the oxidation of organic compounds [8, 16]. Most of the reactions studied were carried out under gas phase heterogeneous catalysis and little has been done to study probable applications in the CWAO reactions.

With this in mind, in the present paper the wet air oxidation of MTBE was carried out over Rh on alumina-ceria with different ceria contents. The effect of the abundance of Ce^{4+}/Ce^{3+} on the rhodium oxidation state, and on the activity and selectivity for the MTBE mineralization was analyzed. The supports were prepared by incorporating cerium nitrate with aluminum boehmite (Catapal B) to improve the interaction of ceria with the alumina. The characterization of the catalysts was performed by means of X-ray diffraction (XRD) spectroscopy; High Angle Annular Dark Field (HAADF) Scanning Transmission Electron Microscopy (STEM), Energy Dispersive X-ray Spectrometry (EDXS) and dehydrogenation of cyclohexane (DCH). The activity was evaluated in the MTBE wet catalytic mineralization.

Experimental Procedure

Preparation of the supports

The γ-Al_2O_3 support was obtained by direct calcination of

*Corresponding author:
Tel : (52) 55 5804 46 68
Fax: (52) 55 5804 4666
E-mail: gdam@xanum.uam.mx

the boehmite Catapal B (CONDEA, high purity 99.999%, 74% Al_2O_3, 26% H_2O) under air flow (3.6 l h^{-1}) at 650 °C for 12 h. The γ-alumina-ceria supports containing 1, 5, 10 and 20 Ce wt%, were prepared by adding the appropriated amounts of an aqueous solution containing $Ce(NO_3)_3$. $6H_2O$ (Strem Chemicals, 99.9%) to the aluminum boehmite Catapal B. Afterwards, the impregnated boehmite was kept under stirring in a rotary evaporator for 4 h. The water excess was evaporated under vacuum at 60 °C and then the solid was dried completely in an oven at 120 °C for 12 hours. Finally, the γ-Al_2O_3-Ce supports were obtained by annealing the samples under an air flow at 650 °C for 24 h.

Preparation of the catalyst

The catalysts were prepared by the wet impregnation ofthe Al_2O_3 and γ-Al_2O_3-Ce supports, with the appropriate amount of an aqueous solution containing $RhCl_3.3H_2O$ (Strem Chemicals 99.99%) to obtain a nominal concentration of 1 wt% of Rh. The catalysts were dried at 120 °C in an oven for 12 h and then calcined under an air flow (3.6 l h^{-1}) at 500 °C for 4 h. Finally, the catalysts were reduced at 500 °C under a hydrogen flow (3.6 l h^{-1}) during 5 h and stored until characterization. The real percentage of Rh on the catalysts was obtained by plasma spectroscopy. The catalysts containing CeO_2 were labeled Rh/ACeX, where X indicates the amount of Ce for each sample, X = 1, 5, 10 and 20 wt%.

BET surface area

The specific surface areas of the catalysts were obtained form the nitrogenadsorption isotherms obtained with a Quantachrome Multistation Autosorb 3B analyzer. Before adsorption, the calcined supports were outgassed at 400 °C under vacuum (1.3 μPa) for 2 h. The specific surface areas were calculated with the BET equation and the mean pore size by the BJH method.

X-Ray measurements

The X-ray diffraction patterns of the supports were obtained to identify the alumina and cerium oxide on the calcined samples. A SIEMENS-D500 diffraction instrument using a Cu Kα radiation and a graphite monochromator in the secondary beam was used. Specimens were prepared by Packing the powdered samples into glass holders. Intensitydata weremeasured bystep scanning through the 2θ rangesbetween 20° to 70° with a 2θ step of 0.02° and a measuring time of 1 s/point. The identification of the XRD peaks was made using JCPDS cards.

XPS spectroscopy studies

The XPS spectra were obtained with a spectrometer model THERMO-VG, ESCALAB 250 equipped with an aluminum anode (energy of 1486.8 eV) and a system monocromator for X Rays of 15 kV and 150 Watts, an energy in passing (Pass energy) of 150 eV and a step size of 1 eV. To correct the landslide of the signs due to the charging effect, the sign 1s of the residual carbon (adventitious coal) at 284.6 eV, was used. The stored reduced samples were placed over a thin sheet of indium and then analyzed. In order to control the sample charge in all experiments, an electron flood gun was used. The analyzed signs were adjusted by using the program ORIGIN FOB version 7.0 and its PEAKFIT module.

STEM and EDXS studies

High angle annular dark field (HAADF) scanning transmission electron microscopy (STEM) analysis of the samples annealed and reduced at 500 °C was performed in a JEM-2200FS Transmission Electron Microscope with an accelerating voltage of 200 kV. The microscope is equipped with a Schottky-type field emission gun and an ultra high resolution (UHR) configuration (Cs = 0.5 mm; Cc 1.1 mm; point-to-point resolution, 0.19 nm) and in-column omega-type energy filter.

Local chemical analysis by Energy Dispersive X-ray spectrometry (EDXS) was performed in a NORAN energy dispersive X-ray spectroscope, which is attached to the microscope using the STEM-EDX combination. The samples were ground, suspended in isopropanol at room temperature, and dispersed with ultrasonic agitation; then, an drop of the solution was placed on a 3 mm diameter holey carbon copper grid.

Cyclohexane dehydrogenation

The catalytic activity of the cyclohexane dehydrogenation was determined at 300 °C, on samples reactivated *in situ* under a H2 flow at 400 °C, using a conventional flow reactor which was set in differential mode (low conversions < 15%). The H_2 flow was fed to a saturator containing the cyclohexane at 12 °C, the mixture of cyclohexane/ hydrogen was passed through the reactor and the products were analyzed by on-line gas chromatography. As for the reaction conditions the partial pressures of cyclohexane and hydrogen were 6.4 and 94.9 Pa respectively. A crosslinked methylsiloxane of 50 m × 0.2 mm × 0.5μm column was used. The activity is expressed as initial specific rate (r_i), $molg_{cat}^{-1}$ $minute^{-1}$ and as initial turnover frequency (TOFi), $minute^{-1}$.

Oxidation reaction conditions

Experiments were carried out in a 300 ml batch reactor (Parr Instrument Co. Ltd., Illinois, U.S.A.), equipped with a valve for sampling, a magnetic driven stirrer, a gas supply system and a temperature controller. The reaction was carried out as follows: 150 ml of a MTBE solution with a concentration of 235 ppm was placed in a glass vessel to avoid the contact of the solution with the reactor and then 1 g l^{-1} of the catalyst was loaded into the reactor. The reactor was firstly purged with nitrogen for 15 minutes and then heated to 120 °C. Afterwards, an oxygen pressure of 10 bars was introduced in the reactor and under continuous stirring (1,000 rpm) the reaction was initiated. Previous calibrations showed that under such conditions the reaction

rate was not controlled by the diffusion of oxygen into the liquid phase.

The evolution of the reaction was followed by performing the analysis of aliquots (on average 1 ml) at intervals of 10 minutes for 1 h. The samples were collected by using the sampling valve, which is equipped with a microspore glass filter to prevent the loss of catalyst.

The samples were analyzed by GC with a FID detector equipped with a capillary column (DB-WAX 30 m × 0.53 mm id, 1.0 μm). A temperature ramp was set up from 80 to 120 °C with a rate of 20 °C minutes^{-1} in order to separate the pollutant and their by-products during the reaction. The by-products were identified by means of a HP-MS-GC 5973. The analysis of total organic carbon (TOC) was performed by using a 5000TOC Shimadzu Analyzer, which was previously calibrated to obtain concentrations in the range of 0 to 300 ppm of TOC. The percentage of the TOC abatement (TOC%) was defined as 100(TOCo-TOC)/TOCo and the percentage of chemical oxygen demand (COD%) as 100(DCOo-DCO)/DCOo. The initial specific rates of conversion (r_i) were calculated from the curves giving the concentration of MTBE as a function of time [10]: $[(\Delta conc/\Delta t)\cdot(MTBE_i/m_{cat})]$ where $(\Delta conc/\Delta t)$ is the initial slop of the concentration curve; $MTBE_i$, initial concentration of the methyl *tert*-butyl ether, m_{cat} the mass of the catalyst, the rate was expressed as mol g_{cat}^{-1} minute^{-1}. The pH and selectivity were measured after 1 h of reaction. The pH was measured using a Conductronic PC-45 and the selectivity to CO_2 (Sco_2) was calculated using the following relationship [17]:

$$Sco_2 = \frac{TOC}{MTBE}\,100 \qquad (1)$$

No leaching of rhodium or alumina was detected. These catalytic systems showed stability in the MTBE oxidizing reaction under the CWAO conditions used in this study.

Results and Discussion

Specific surface area

The specific surface area for the boehmite reference was 220 m^2g^{-1}. The calcination of the boehmite at 650 °C led to obtain a γ-Al2O3 support with a specific surface area of 173 m^2g^{-1}. For the alumina support samples containing cerium, the specific surface areas diminishes, since these supports were obtained by impregnation of the boehmite with a Ce nitrate solution and then calcined at 650 °C. The BET areas calculated were 164, 156, 157 and 128 m^2g^{-1} for the γ-Al_2O_3-Ce supports with loads of 1, 5, 10, and 20 Ce wt%, respectively. A wide Ce contact with the alumina support and important modifications in their textural properties can be then expected. The analysis of the porosity of these materials showed mesopore size distributions and the mean pore size was found to be around 6.8-7.5 nm.

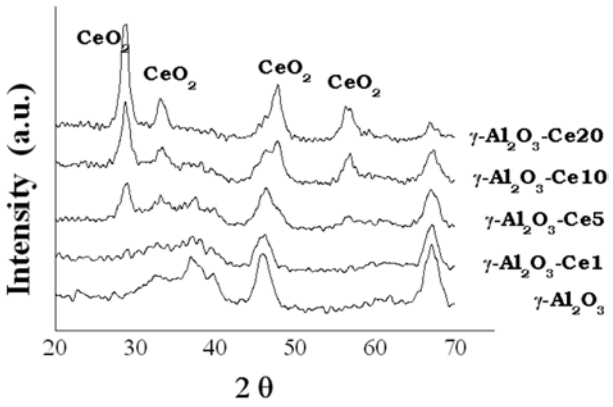

Fig. 1. XRD spectra for the various supports.

X-ray-Diffraction

The X ray diffraction spectra of the supports showed theformation of γ-Al_2O_3. For the ACe1 support only the characteristic peaks of γ-Al2O3 were observed. Meanwhile, for the supports with 5, 10 and 20 wt% Ce the characteristic peaks of cerium oxide could be observed and their intensity increases with the Ce content, Fig 1. The identification by XRD of important amounts of cerium oxide on the alumina supports with high cerium contents is probably the cause of the specific surface area diminution showed by these supports.

X-ray photoelectron spectroscopy.

The XPS spectra for the Rh/A and Rh/ACeX were studied in air-exposed catalysts, since the MTBE oxidation reaction would be carried out in an oxygen environment. In Fig. 2 the XPS of the Rh $3d_{5/2}$ core level of the deconvoluted spectra are showed. Two binding energies (B.E.) that appear at around 306.9-307.5 eV and 308.4-309.0 eV, assigned to the Rh^o and $Rh^{\delta+}$ species respectively can be observed [18, 19]. In Table 1, the binding energies and their relative abundance (numbers in parentheses)

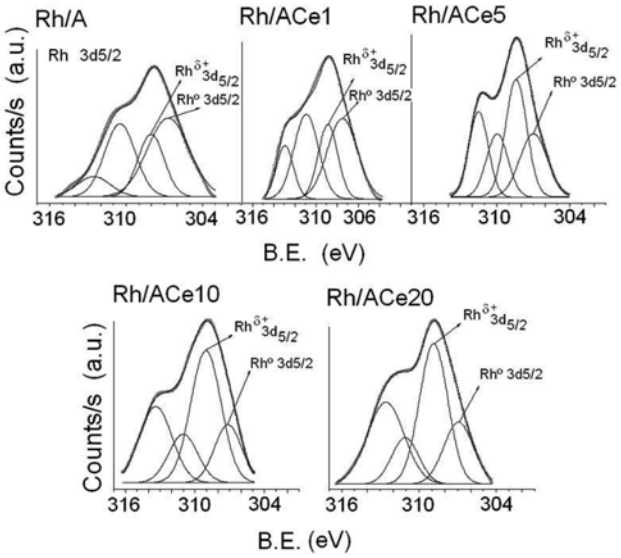

Fig. 2. XPS spectra for the Rh $3d_{5/2}$ region for Rh catalysts.

Table 1. Binding energy (B.E.) of $Rh3d_{5/2}$ and $Ce3d^{5/2}$ and percentage of Rh^o, $Rh^{\delta+}$ and Ce^{3+}, Ce^{4+} for Rh catalysts

Catalyst	Species	Rh $3d_{5/2}$ (eV)	Species	Ce $3d_{5/2}$ (eV)
Rh/A	Rh^o (71)	307.5	-	-
	$Rh^{\delta+}$ (29)	309.0	-	-
Rh/ACe1	Rh^o (65)	307.5	Ce^{3+} (52)	884.6, 887.9
	$Rh^{\delta+}$ (35)	308.8	Ce^{4+} (48)	890.7, 900.9
Rh/ACe5	Rh^o (43)	306.9	Ce^{3+} (37)	881.9, 885.3
	$Rh^{\delta+}$ (57)	308.4	Ce^{4+} (63)	887.6, 898.7
Rh/ACe10	Rh^o (31)	307.1	Ce^{3+} (34)	882.0, 885.2
	$Rh^{\delta+}$ (69)	309.0	Ce^{4+} (66)	887.2, 899.1
Rh/ACe20	Rh^o (30)	306.9	Ce^{3+} (27)	882.2, 884.7
	$Rh^{\delta+}$ (70)	308.9	Ce^{4+} (73)	886.8, 897.2

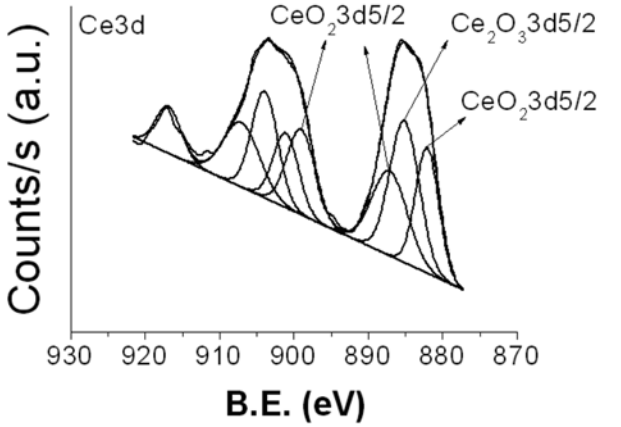

Fig. 3. XPS spectrum for the Ce 3d region for Rh/ACe10 catalyst.

for the Rh^o and $Rh^{\delta+}$ species are reported. The lowest proportion of $Rh^{\delta+}$ was obtained in the parent catalyst Rh/A (29%) and it increases to 35, 57, 69 and 70 in the catalysts containing cerium oxide with 1, 5, 10 and 20% Ce respectively. In the deconvoluted spectra, Fig. 2, the peaks at higher binding energies corresponding to the Rh $3d_{3/2}$ core level can also be observed. Several researchers have experienced the complexity of the Ce 3d spectra; we have taken into account the experience of other authors to perform the deconvolution and assignation of the peaks [20-22]. All the Ce-containing samples exhibited the Ce $3d_{5/2}$ and $3d_{3/2}$ characteristic peaks. For the calculation of the relative abundance of Ce^{3+} and Ce^{+4}, $3d_{5/2}$ energy level, the peaks in the range of the binding energies of 881.9-887.9 eV and 886.8-900.9 eV, which correspond to the Ce^{3+} and Ce^{4+} oxidized states, respectively, were deconvoluted [18]. In Fig. 3 is presented as an example the XPS spectra of the decomposed Ce 3d peaks for the Rh/ACe10 catalyst. In Table 1, the binding energy, BE, for Ce $3d_{5/2}$, as well as the proportion of each species in the catalysts (in parentheses) are reported. A reduction of the abundance of Ce^{3+} with the loading of cerium in the catalysts is observed. The increase of the $Rh^{\delta+}$ species with the loading of Ce is related to a high interaction between Rh and ceria which stabilize this species [20, 23]. On the other hand,

Table 2. Surface atomic ratios for alumina and alumina-ceria supported Rh catalysts

Catalyst	Rh/Al	Ce/Al	Rh/Ce
Rh/A	0.00512	-	-
Rh/ACe1	0.00511	0.00358	1.428
Rh/ACe5	0.00532	0.01870	0.280
Rh/ACe10	0.00542	0.03309	0.160
Rh/ACe20	0.00589	0.05518	0.1067

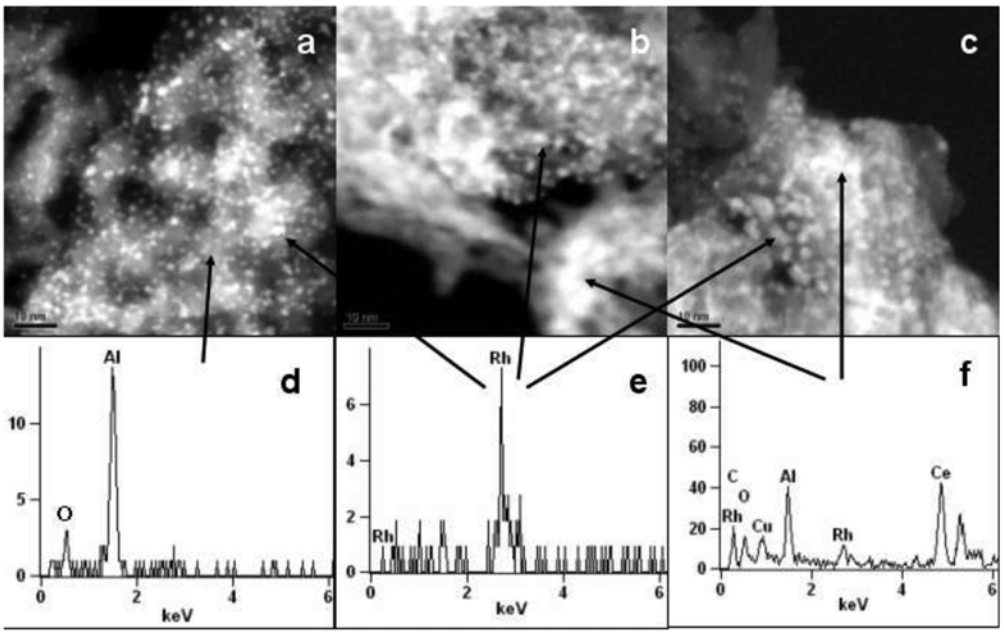

Fig. 4. HAADF-STEM image of the samples a)Rh/A, b)Rh/ACe10 and c)Rh/ACe20 showing the dispersion and size of the nanoparticles on the support. EDXS spectra corresponding to, d) alumina support (gray region) e) white nanoparticle and f) alumina and ceria support (white region, sample with 20 wt% of Ce).

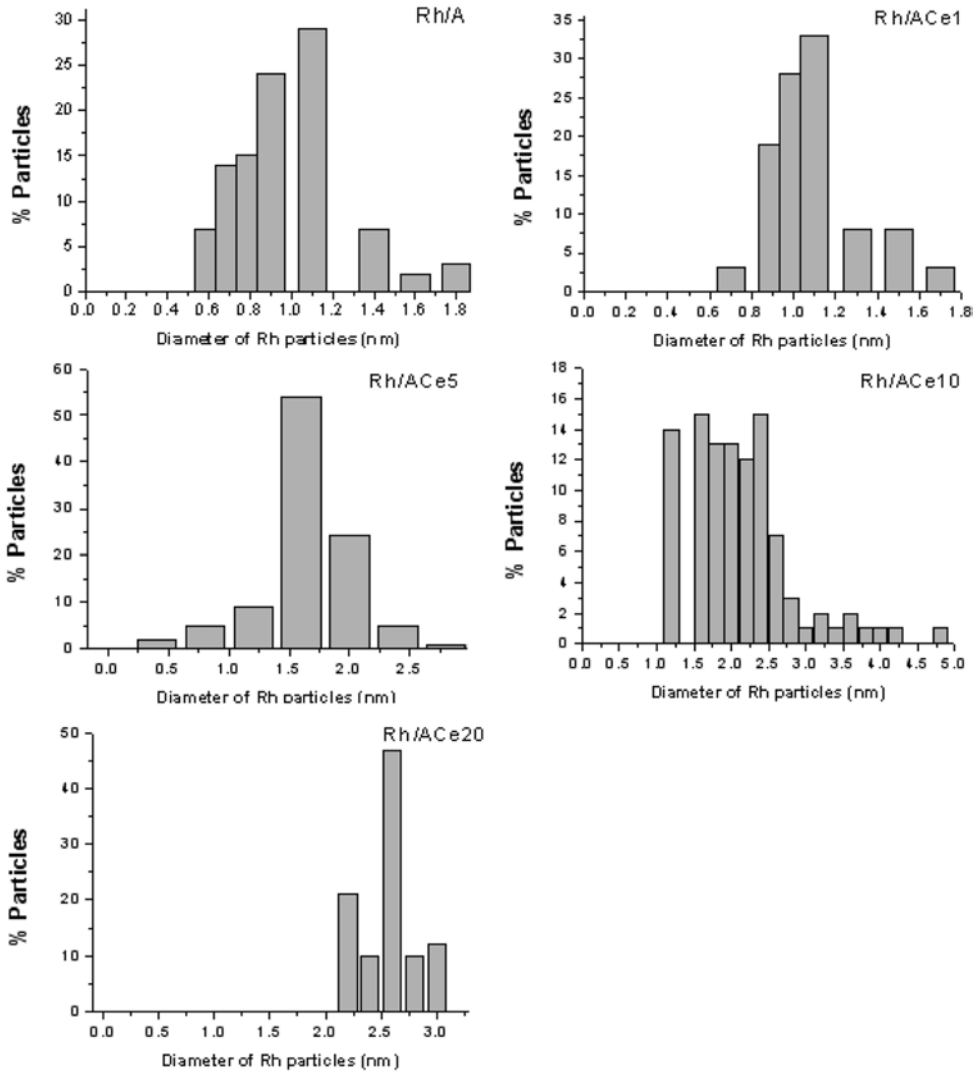

Fig. 5. Metal particle size histograms of for the different rhodium catalysts.

the high proportion of Ce^{4+} as a function of the Ce content on the surface layer is not surprising since the XPS measurements were performed on samples which were not pre-reduced "in situ" in the XPS chamber. The reaction occurring after exposure to air is $Ce^{3+} + O_2 \rightarrow Ce^{4+} + H_2O$. We will determine the MTBE degradation under oxidizing conditions in air exposed catalysts, then the XPS results obtained on the unreduced samples will reflect more accurately the surface composition of the catalysts used in the MTBE oxidation.

The surface atomic ratios Rh/Al, Ce/Al and Rh/Ce are reported in Table 2. The Rh/Al ratio increases as the cerium content does, meanwhile the inverse effect, a diminution in the Rh/Ce ratio is observed, this means that the amount of Ce increases on the alumina surface although, it can not be excluded that the enhanced signal from surface Ce just comes from the pure phase of ceria present in the alumina-ceria mixed metal oxide system.

STEM and EDX studies

Figs. 4a, 4b and 4c show the HAADF-STEM images of three selected samples Rh/A, Rh/ACe10 and Rh/ACe20 respectively, where rhodium nanoparticles it can be seen on the support. The corresponding histograms and particle size distributions are showed in Fig. 5. The mean particle size was calculated with the expression $d = \sum n_i d_i^3 / \sum n_i d_i^2$ where d is the mean particle size, d_i is the diameter measured directly from the electron micrographs and n_i is the number of particles having the diameter d_i (Table 3). Particle size ranging from 1.0 to 2.5 nm were obtained. The samples showing the highest dispersion are those containing 1 and 5% Ce (< 1.5 nm); whereas the samples with higher loads, 10 and 20 wt% Ce are at around 2.3 and 2.5 nm respectively.

On the other hand, the EDSX analyses of the selected catalysts are shown in Figs. 4d, 4e and 4f. For the Rh/A sample in the gray regions only aluminum and oxygen were detected, meanwhile in the white region only Rh was detected. On the other hand, the analysis of the white contrast region showed the presence of Al, O, Ce and Rh suggesting that the Rh nanoparticles are surrounding cerium oxide, (Fig. 4f). However, it is not possible to

Table 3. Characterization of Rh supported on γ-Al_2O_3 and γ-Al_2O_3-Ce catalysts

Catalyst	[1]Rh wt%	Cl wt%	Cl/Rh	[2]d (nm)	[2]Metal area $m^2\ g_{cat}^{-1}$	[2]D%	[3]$r_i \times 10^5$ $molg_{cat}^{-1}\ minute^{-1}$	[3]$TOF_i\ minute^{-1}$
Rh/A	0.7	1.2	3.7	1.0	3.1	100	1.1	16
RhACe1	0.74	1.1	4.1	1.1	3.2	98	1.2	17
Rh/ACe5	0.78	1.2	4.2	1.5	2.5	72	1.0	18
Rh/ACe10	0.89	1.5	4.5	2.3	1.8	46	0.8	19
Rh/ACe20	0.99	1.6	4.9	2.5	1.9	43	0.6	14

[1]Determined by ICP Spectroscopy. [2]Obtained by High Angle Annular Dark Field (HAADF) Scanning Transmission Electron Microscopy (STEM). [3]Cyclohexane Dehydrogenation at t = 0.

deduce whether rhodium is preferentially placed on ceria or alumina conglomerates, neither whether Rh was covered by cerium oxide or not. Based on the information of the mean particle size (*d*) obtained by HAADF-STEM, the metal area and the dispersion of rhodium (D%) were calculated, see Table 3. The metallic areas were expressed as $m^2g_{cat}^{-1}$ and the number of rhodium atoms on a surface has been calculated assuming $1.33 \cdot 10^{19}$atoms of rhodium per square metre [24].

Cyclohexane dehydrogenation

The catalytic activity of the cyclohexane aromatization measured at 300 °C is reported in Table 3. This insensitive structure reaction has been reported as a plausible option to determine the active metal surface area in cerium containing catalysts [25]. The results reported in Table 3 show that the specific rate for the cyclohexane dehydrogenation (r_i) diminishes as the cerium content increases. Specific activities of 1.2, 1.0, 0.8 and 0.6 mol g_{cat}^{-1} $minute^{-1}$ were obtained on the catalysts containing 1, 5, 10 and 20 Ce wt%, respectively. If we take into account the fact that the activity for this insensitive reaction is proportional to the number of active atoms on the surface, we can say that the specific rate varies almost in the same proportion as the metal dispersion. These results are in good agreement with those obtained by HAADF-STEM. On the other hand, the activity per site (turn over frequency, TOF) was also calculated from the specific activity and from the Rh particle size determined by HAADF-STEM (Table 3). The Rh/A catalyst present a TOF value of 16 $minute^{-1}$, whereas as for the catalysts containing cerium, the values are comprised between 14 to 19 $minute^{-1}$. These values did not go far from an average factor of 1.3; which can be considered, to be in the range of experimental error. Therefore, it can be considered that the TOF is practically constant which confirms the insensitivity of the cyclohexane dehydrogenation reaction. We can say that the number of Rh active sites determined by this way is valuable and then it can be used to calculate the TOF for the MTBE degradation.

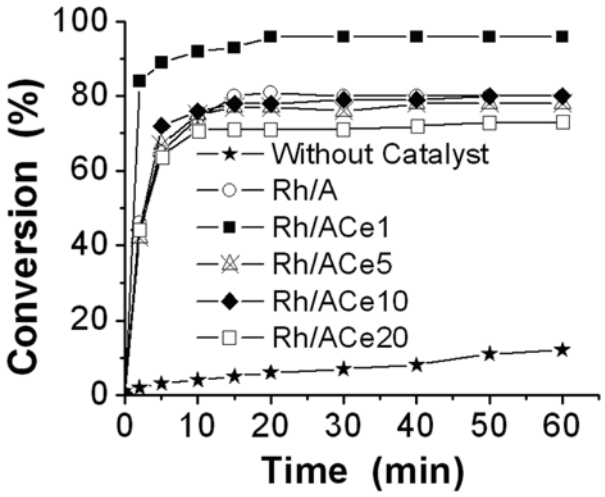

Fig. 6. MTBE conversion during the oxidation at 120 °C for the different Rh/ACeX catalysts.

MTBE Oxidation

The MTBE oxidation as function of time at 120 °C is presented in Fig. 6. As can be seen, the conversion for the non-catalyzed reaction reaches 11% after 1 h, meanwhile, the catalyzed MTBE wet oxidation showed higher conversions (Table 4). Conversions ranging from 96 to 73% depending on the Ce content in the catalysts were obtained. The maximum conversion corresponds to the Rh/ACe1 (96%) and the lowest one to the Rh/ACe20 (73%) catalysts, meanwhile, conversions ranging between 78-80% were obtained with the bare Rh/A, Rh/ACe5 and RhACe10. In the liquid phase, the evolution of the

Table 4. Cerium effect in activity and selectivity to CO_2 on Rh/Al_2O_3-CeX catalysts, after 1 h of reaction at 120°C

Catalyst	Conversion (%)	TOC Abattement (%)	COD Abattement (%)	CO_2 (%)	pH	$r_i \times 10^3$ $molg_{cat}^{-1}\ minute^{-1}$	TOF_i $minute^{-1}$
Rh/A	80	50	81	65	4.9	6.1	91
Rh/ACe1	96	72	84	75	6.9	8.4	118
Rh/ACe5	78	55	77	73	5.6	5.5	101
Rh/ACe10	80	62	67	79	5.8	2.6	65
Rh/ACe20	73	64	75	87	5.6	3.1	76

reaction as a function of time, in most cases, is difficult to interpretation since the reactants and products are in the same reactant medium. Inhibition or auto catalysis effects due to the presence of the products can occur. To avoid such a problematic situation, it is preferable to determine the activity at an initial specific rate obtained by extrapolating the evolution curves as a function of time. The values of the initial specific rate showed a constant diminution as a function of the cerium content in the catalysts. The initial specific rates for the MTBE oxidation (Table 4) were 8.4 5.5, 2.6 and 3.1 mol g_{cat}^{-1} $minute^{-1}$ for the catalysts with cerium loadings of 1, 5, 10 and 20 wt% respectively. This behavior can be related to the relative Rh^o:$Rh^{\delta+}$ abundance (Table 1). The maximum in the activity was obtained in the Rh/ACe1 catalyst showing an optimal 65 : 35 ratio. For high cerium contents the catalysts showed a lower activity and a higher $Rh^{\delta+}$ abundance (57-70%). It is important to note that in the bare Rh/A catalyst a higher Rh^o:$Rh^{\delta+}$ ratio (71 : 29) was identified by XPS, however, its specific rate (6.1 mol g_{cat}^{-1} $minute^{-1}$) is comparable with that obtained on the Rh/ACe5 catalyst (5.5 mol g_{cat}^{-1} $minute^{-1}$). The activity of the bare Rh/A catalyst could be associated to the high abundance of Rh^o in the reduced state, and then we can assume that the mechanism by which the MTBE oxidation occurs in this catalyst is different to that observed in catalysts containing cerium. The activity expressed as TOF (calculated in the same way used for the cyclohexane dehydrogenation) for the MTBE conversion is reported in Table 4, which did not show any appreciable variation for the different catalysts; although the Rh/ACe1 showed the highest activity. It has been reported that large metal particles are the most active for the oxidation of organic compounds [10]. However, our results show that the domain of particle size for the different catalysts is around 1.0-2.5 nm. The effects of particle size on rhodium catalysts have been observed when the metallic particles are larger than 3.0-5.0 nm [26-28]. Then, it is difficult to detect particle size effects on the MTBE oxidation in our rhodium alumina-ceria supported catalysts. The total oxidation of MTBE was followed as indicated above. According to the data obtained by XPS concerning fresh samples containing cerium, we assume that the following reactions can be occurring in the reactor in the presence of a reducer such as MTBE and an oxidizing agent as oxygen. The active site for MTBE is the $Rh^{\delta+}$ which is reduced and re-oxidized in the course of the reaction:

$$Ce^{3+} + O_2 \rightarrow Ce^{4+} + H_2O \quad (2)$$

$$Ce^{4+} + Rh^o \rightarrow Ce^{3+} + Rh^{\delta+} \quad (3)$$

$$Rh^{\delta+} + \text{MTBE} \rightarrow Rh^o + CO_2 + H_2O \quad (4)$$

One of the most important results is to get the total mineralization of the reactant. In Table 4 the mineralization to CO_2 is reported for the various catalysts. The results show that the formation of CO_2 strongly depends on the cerium content in the alumina support. This varies from 65% CO_2 for the bare Rh/A catalyst to 87% CO_2 for the catalyst containing the highest Ce content (Rh/ACe20). The positive effect of cerium oxide on the catalysts for the MTBE oxidation can be clearly seen in the high mineralization values obtained. The conversion level in some cases can modify the formation of CO_2, then, by comparing the Rh/A bare catalyst with the Rh/ACe10 catalyst, which shows the same conversion level (80%) for the former, the mineralization (CO_2%) was 65, whereas for the latter was 79%. In Fig. 7, is shown a correlation of the formation of CO_2 with the relative abundance of Ce^{4+}/Ce^{3+} (Table 1). At high Ce^{4+}/Ce^{3+} ratios, the oxidation of the organic compound was lowest, but the highest selectivity to the mineralization was obtained. In Table 4, the values for TOC and COD abatements are also reported. It can be seen that the Rh/ACe1 catalyst shows the highest total organic carbon TOC abatement with 72% which is in good agreement with the maximum chemical oxygen demand COD abatement of 84%. The differences between conversion and mineralization indicate that some organic intermediates are formed and they remain in the reactant solution. The pH of the starting solution and after 1 h in reaction conditions was determined. The MTBE pH in an aqueous solution was 5.0, while after 1 h of reaction it increased to 5.6-6.9 depending on the cerium content over the Rh/ACeX catalysts. An acceptable correlation between the MTBE conversion and the pH can be observed, by comparing the pH values (Table 4) and the MTBE conversion as a function of time (Fig. 8). In fact, the highest pH of the solution after the MTBE degradation corresponds to the catalyst Rh/ACe1 which showed the highest activity. As for the other cerium catalysts, a similar variation in the pH (5.6-5.8) and in conversion (73-78 %) was obtained. In the bare catalyst the pH in the solution, after 1 h of reaction, was practically the same (4.9) as that MTBE in aqueous solution, even when its activity reaches 80%. The explanation to this singular behavior certainly resides in the by-products formed on this catalyst as will be

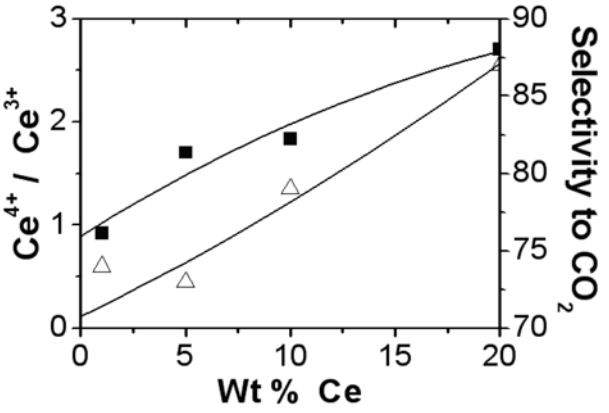

Fig. 7. Effect of the Ce^{4+}/Ce^{3+} abundance in the mineralization to CO_2 of the MTBE oxidation over Rh/ACeX catalysts: Ce^{4+}/Ce^{3+} (■), Selectivity to CO2 (△).

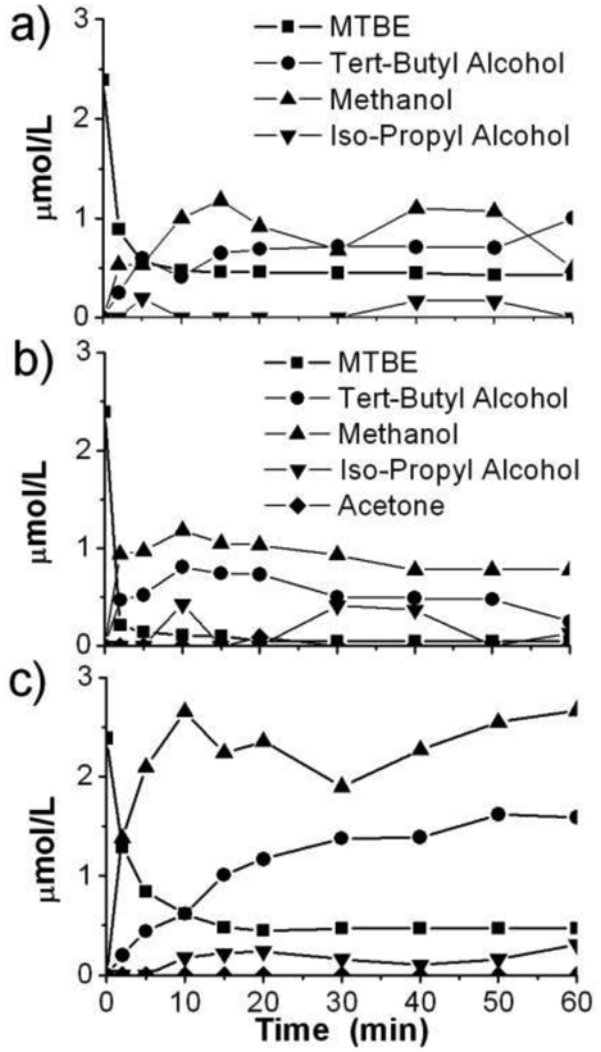

Fig. 8. Concentration profile of intermediates and MTBE for selected catalysts during the oxidation at 120°C: a) Rh/ACe20, b) Rh/ACe1, c)Rh/A.

discussed below. It was found that the oxidation of MTBE on Rh catalysts at 120°C was accompanied by the formation of various by-products. They were identified by means of MS-GC as *tert*-butyl alcohol, methanol, *iso*-propyl alcohol and acetone. In Fig. 8 concentration-time profiles of these by-products during the MTBE oxidation for the Rh/A, Rh/ACe1 and Rh/ACe20 catalysts are shown. According to the results shown in Fig 8, the pathway for the MTBE oxidation should be similar in Ce free and in the Ce containing catalysts (Fig. 9). However, due to the oxidizing capacity of the Ce^{4+}/Ce^{+3} redox pair, the *tert*-butyl alcohol, methanol, *iso*-propyl alcohol and acetone oxidation must be achieved faster in catalysts containing cerium than in the catalyst free of Ce. This assumption is supported by Fig. 8c where it can be clearly seen that the amount of methanol as well as *tert*-butyl alcohol is double of that quantified in cerium catalysts. The efficiency for the total oxidation (TOC) is reported in Table 4 where the highest TOC values correspond to the catalysts containing cerium oxide.

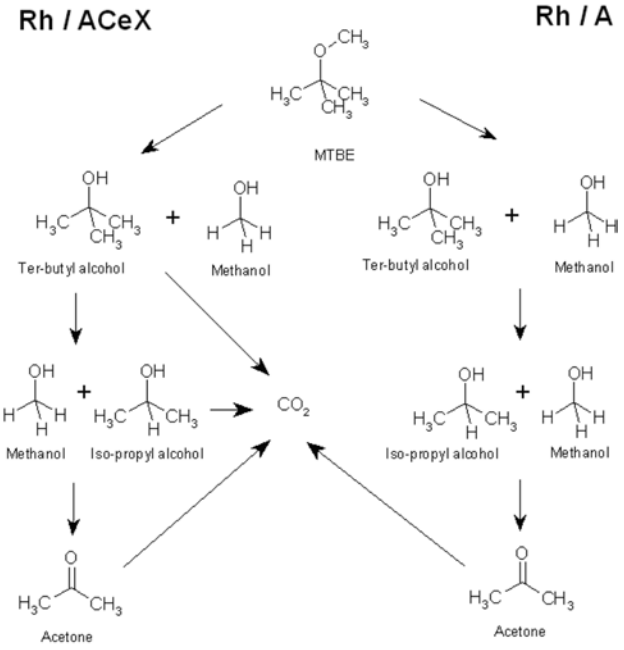

Fig. 9. The proposed pathway for MTBE oxidation.

Conclusions

The addition of cerium nitrate to boehmite forms mixed oxides with high concentrations of cerium oxide over the alumina support. Small rhodium particle sizes were found by High Angle Annular Dark Field (HAADF) Scanning Transmission Electron Microscopy (STEM). As for Rh impregnated supports, the XPS study showed that cerium oxide stabilizes the formation of $Rh^{\delta+}$ species and the Ce^{4+}/Ce^{3+} redox pair. It is shown that for the MTBE oxidation it is of great importance the effect of the Ce^{4+}/Ce^{3+} pair is of great importance in the total mineralization of the reactant. We can say that the higher the Ce^{4+}/Ce^{3+} ratio, the higher the total mineralization is.

Acknowledgements

We acknowledge CONACYT for the support provided to the Project SEP-2004-COI-46689Q. I. Cuauhtémoc and J.M. Padilla thank CONACYT for the grants awarded.

References

1. R. Johnson, J. Pankow, D. Bender, C. Price and J. Zagorski, Environ. Sci. Technol. Feature 34 (2000) 210A-217A.
2. M. Anderson, Environ Sci. Technol. 34 (2000) 725-727.
3. M. Mitani, A.A. Keller, A. Burton, R. Rinker and O. Sandall, J. Hazardous Materials B89 (2000) 197-212.
4. V.S. Misha, V.V. Mahajani and B. Joshi, Ind. Eng. Chem. Res. 34 (1995) 2-48.
5. J. Levec and A. Pintar, Cat. Today, 124 (2007) 172-184.
6. J. Levec and A. Pintar, Catal. Today 24 (1995) 51-58.
7. S.I. Imamura, I. Fukuda and S. Ishida, Ind. Eng. Chem.

Res. 27 (1988) 718-726.
8. L. Oliviero, J. Barbier, Jr., D. Duprez, H. Wahyu, J.W. Ponton, I.S. Metcalfe and D. Mantzavinos, Appl. Catal. B 35 (2001) 1-12.
9. L. Olivierio, J. Barbier, Jr., S. Labruquere and D. Duprez, Catal. Lett. 60 (1999) 15-19.
10. J. Barbier, Jr., L. Oliviero, B. Renard and D. Duprez, Top. Catal. 33 (2005) 77-86.
11. J.C. Beziat, M. Besson, P. Gallezot and S. Durecu, J. Catal. 182 (1999) 129-135.
12. M. Besson and P. Gallezot, Top. Catal. 33 (2005) 101-108.
13. Y. Harada and K. Yamasaki, Desalination 98 (1994) 27-39.
14. A. Pintar and J. Levec, Chem. Eng. Sci. 47 (1992) 2395-2400.
15. J. Levec and A. Pintar, Cat. Today 24 (1995) 51-58.
16. F. Sadi, D. Duprez, F. Gerard and A. Miloudi, J. Catal. 213 (2003) 226-234.
17. S. Ling, D.J. Chang and C.H. Wang, Water Res. 37 (2003) 793-800.
18. J.F. Moulder, W.W. Stickle, P.E. Sobol and K.D. Bomber, in Hand book of X-ray photoelectron spectroscopy, Ed. J. Chastain, Perkin Elmer, Eden Praine, U.S.A., (1978) p.108.
19. G. Pecchi, P. Reyes, R. Gòmez, T. Lòpez and J.L.G. Fierro, Appl. Catal. B: Env. 17 (1998) L7-L13.
20. A. Gayen, K.R. Priolkar, P.R. Sarode, V. Jayaram, M.S. Hedge, G.N. Subbanna and S. Emura, Chem. Mater. 16 (2004) 2117-2328.
21. J.C. Conesa, M. Fernandez-Garcia and A. Martinez Arias, in Catalysis by Ceria and related Materials, Chapter 5, Ed. A. Trovarelli, Imperial collage Press, London, (2002) p 169-216.
22. P. Burrougs, A. Hammett, A.F. Orchard and G. Thornton, J. Chem. Soc., Dalton Trans. 17 (1976) 1686-1698.
23. A. Trovarelli, G. Dolcetti, C. Leitenburg, J. Kaspar, P. Finetti and A. Santoni, J. Chem. Soc., Faraday Trans. 88[9] (1992) 1311-1319.
24. J.R. Anderson, In Structure of Metallic Catalysts, Academic Press: London, (1975) pp 296.
25. E. Rogermond, N. Essayem, R. Frety, V. Perrichon, M. Primet and F. Mathis, J. Catal. 166 (1997) 229-235.
26. M.B. Gordon, F. Cyrot-Lackmann and M.C. Desjonquières, Surf. Sci. 68 (1977) 359-367.
27. Yacaman, D. Romeu, S. Fuentes and J.M. Domínguez, Surf. Sci. 106 (1981) 472-477.
28. G. Del Angel, B. Coq and F. Figueras, Nouv. J. Chim. 7 (1983) 173-179.